Progress in Natural Science: Materials International 26 (2016) 477–482

HOSTED BY

ELSEVIER

Contents lists available at ScienceDirect

Progress in Natural Science: Materials International

journal homepage: www.elsevier.com/locate/pnsmi

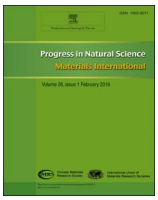

Original Research

Effects of doping in 25-atom bimetallic nanocluster catalysts for carbon–carbon coupling reaction of iodoanisole and phenylacetylene

Zhimin Li[a,b], Xiujuan Yang[a], Chao Liu[a], Jin Wang[a], Gao Li[a,*]

[a] Gold Catalysis Research Center, State Key Laboratory of Catalysis, Dalian Institute of Chemical Physics, Chinese Academy of Sciences, Dalian 116023, China

[b] University of Chinese Academy of Sciences, Beijing 100049, China

ARTICLE INFO

Keywords:
Au_{25} nanocluster
Carbon–carbon coupling reactions
Doping effects
Silver
Copper
Platinum

ABSTRACT

We here report the catalytic effects of foreign atoms (Cu, Ag, and Pt) doped into well-defined 25-gold-atom nanoclusters. Using the carbon-carbon coupling reaction of *p*-iodoanisole and phenylacetylene as a model reaction, the gold-based bimetallic $M_xAu_{25-x}(SR)_{18}$ (–SR=–SCH_2CH_2Ph) nanoclusters (supported on titania) were found to exhibit distinct effects on the conversion of *p*-iodoanisole as well as the selectivity for the Sonogashira cross-coupling product, 1-methoxy-4-(2-phenylethynyl)benzene). Compared to $Au_{25}(SR)_{18}$, the centrally doped $Pt_1Au_{24}(SR)_{18}$ causes a drop in catalytic activity but with the selectivity retained, while the $Ag_xAu_{25-x}(SR)_{18}$ nanoclusters gave an overall performance comparable to $Au_{25}(SR)_{18}$. Interestingly, $Cu_xAu_{25-x}(SR)_{18}$ nanoclusters prefer the Ullmann homo-coupling pathway and give rise to product 4,4′-dimethoxy-1,1′-biphenyl, which is in opposite to the other three nanocluster catalysts. Our overall conclusion is that the conversion of *p*-iodoanisole is largely affected by the electronic effect in the bimetallic nanoclusters' 13-atom core (i.e., Pt_1Au_{12}, Cu_xAu_{13-x}, and Au_{13}, with the exception of Ag doping), and that the selectivity is primarily determined by the type of atoms on the M_xAu_{12-x} shell (M=Ag, Cu, and Au) in the nanocluster catalysts.

1. Introduction

Bimetallic nanoclusters have played a very important role in homogeneous and heterogeneous catalysis due to the synergy between the constituent elements [1–4]. Even more, sometimes the bimetallic nanoclusters could exhibit much better catalytic activities than do the monometallic counterparts [5–9]. The catalytic properties of bimetallic nanocatalysts are influenced by the distribution of the two metallic components in the bimetallic nanoclusters; for example, the alloy, core-shell, and dumb-bell nanostructures behave very differently in catalytic processes [10]. Recently, Kobayashi et al. have reported that the two carbon-stabilized polymer incarcerated gold-based bimetallic nanoclusters catalysts (PI-CB/Au-Pt and PI-CB/Au-Pd) showed very different selectivity in the aerobic oxidation of alcohols and direct oxidative ester formation due to the different structures of the bimetallic nanoclusters [11].

Metal-catalyzed (i.e., Cu, Pd, and Au) carbon–carbon coupling reactions, such as Ullmann homo-coupling and Songashira cross-coupling reactions that result in the formation of new carbon–carbon bonds, are of paramount importance in synthetic organic chemistry [12–16]. Some bimetallic and trimetallic nanoclusters have been reported to be good catalysts for the Songashira cross-coupling reaction [17,18]. Santhanalakshmi's group have reported that the Au/Ag/Pd core/dual-shell trimetallic nanoclusters are applied in the Songashira cross-coupling reaction and the trimetallic nanoclusters showed better catalytic activity than the corresponding mono- and bimetallic nanocluster catalysts [17].

In our previous work, we have reported that the oxide-supported gold nanoclusters ($Au_{25}(SR)_{18}$, where R=CH_2CH_2Ph, hereafter) catalysts were well applied for the Ullmann homo-coupling of aryl iodides and Songashira cross-coupling reactions between *p*-iodoanisole and phenylacetylene [18–22]. It also has been reported that copper and platinum nanoclusters could also be applied for the Ullmann homo-coupling and Songashira cross-coupling reactions in the literatures [12–16]. To gain insight into the fundamental relationship between metal composition of bimetallic catalysts and their catalytic activity/selectivity, we intentionally introduce foreign atoms (e.g., Pt, Ag, and Cu) into the $Au_{25}(SR)_{18}$ nanoclusters and then investigate the catalytic performance of bimetallic catalysts.

Peer review under responsibility of Chinese Materials Research Society.

* Corresponding author.
E-mail address: gaoli@dicp.ac.cn (G. Li).

http://dx.doi.org/10.1016/j.pnsc.2016.09.007
Received 31 July 2016; Accepted 16 August 2016
Available online 13 October 2016

1002-0071/ © 2016 Chinese Materials Research Society. Published by Elsevier B.V. This is an open access article under the CC BY-NC-ND license (http://creativecommons.org/licenses/by/4.0/).

2. Experimental

2.1. Characterization

MALDI mass spectrometry was performed with a PerSeptive Biosystems Voyager DE super-STR time-of-flight (TOF) mass spectrometer. Trans-2-[3-(4-tert-butylphenyl)-2-methyl-2-propenyldidene] malononitrile was used as the matrix in MALDI-MS analysis. Typically, 0.1 mg matrix and 10 μL analyte stock solution were mixed in 10 μL CH_2Cl_2. 10 μL solution was applied to the steel plate and then dried under vacuum (at room temperature) prior to MALDI mass spectrometry analysis. X-ray photoelectron spectroscopy (XPS) analysis was performed on VG ESCAB mk-2.

2.2. Preparation of 1 wt% $M_xAu_{25-x}(SR)_{18}/TiO_2$

$M_xAu_{25-x}(SR)_{18}$ clusters were synthesized according to a literature procedure [23]. Typically, 1 mg $M_xAu_{25-x}(SR)_{18}$ nanoclusters were dissolved in 5 mL DCM, and 100 mg TiO_2 oxides were added. After stirred for 12 h at room temperature, the supernatant became colorless. The $M_xAu_{25-x}(SR)_{18}/TiO_2$ catalysts were collected by centrifugation and dried in vacuum at room temperature The as-prepared $M_xAu_{25-x}(SR)_{18}/TiO_2$ catalysts were then heated to 150 °C in vacuum for 2 h for annealing.

2.3. Typical procedure for carbon–carbon coupling reaction

In a typical carbon–carbon coupling reaction, *p*-iodoanisole (0.1 mmol), phenylacetylene, K_2CO_3 (0.3 mmol), $M_xAu_{25-x}(SR)_{18}/TiO_2$ (100 mg) (the catalysts should be activated at 150 °C in vacuum for half hour before the reaction) and 1 mL DMF were added to a 5 mL one-neck round-bottom flask. The mixture was stirred under N_2 atmosphere at 160 °C for 40 h as indicated in Table 1. After the reaction, 10 mL water was added to the flask, followed by extraction with EtOAc (2 mL×2). The products were obtained after removing EtOAc. The products were characterized by proton nuclear magnetic resonance (^{1}H NMR) spectroscopy. The conversion of *p*-iodoanisole and yields of 4,4′-dimethoxy-1,1′-biphenyl and 1-methoxy-4-(2-phenylethynyl)benzene were determined by NMR (300 MHz) analysis.

Table 1
The catalytic performances of TiO_2-supported $M_xAu_{25-x}(SR)_{18}$ nanocluster catalysts for the carbon–carbon coupling reaction between *p*–iodoanisole and phenylacetylene.[a]

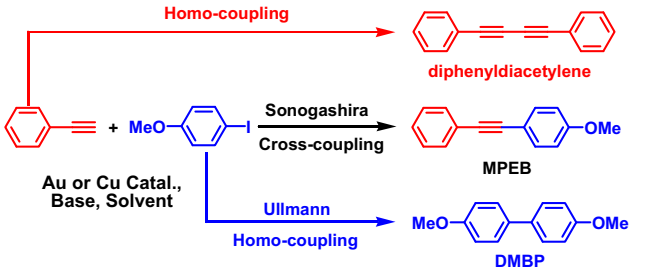

Entry	Catalysts	Conversion [%][b]	Selectivity [%][b]	
			MPEB	DMBP
1	$Au_{25}(SR)_{18}$	79.5	65.7	34.3
2	$Ag_xAu_{25-x}(SR)_{18}$	83.0	55.4	44.6
3	$Cu_xAu_{25-x}(SR)_{18}$	52.4	28.3	71.7
4	$Pt_1Au_{24}(SR)_{18}$	48.5	67.2	32.9

[a] Reaction conditions: 100 mg catalyst, 1 wt% $M_xAu_{25-x}(SR)_{18}$ loading, 0.1 mmol *p*–iodoanisole, 0.1 mmol phenylacetylene, 0.3 mmol K_2CO_3, 1 mL DMF, 160 °C, 40 h.
[b] The conversion of *p*–iodoanisole and selectivities for DMBP and MPEB were determined by ^{1}H NMR.

3. Results and discussion

3.1. Characterization of the three different gold-based bimetallic nanoclusters

The synthesis of the three different gold-based bimetallic nanoclusters followed the literature protocols [6,23], e.g., single-atom Pt doped $Pt_1Au_{24}(SR)_{18}$ nanoclusters, multiple-atom doped $Cu_xAu_{25-x}(SR)_{18}$ (x=0 to 6) and $Ag_xAu_{25-x}(SR)_{18}$ (x=0 to 5). And we also synthesized as well as homogold $Au_{25}(SR)_{18}$ nanoclusters [24,25] for comparison. All the nanoclusters were firstly characterized and determined by matrix-assisted laser desorption/ionization (MALDI)-mass spectrum (Fig. 1).

The MALDI mass spectrum of $Au_{25}(SR)_{18}$ nanocluster exhibits an intense peak at m/z 7394 Da (where z=1) corresponding to the calculated formula weight of 7394 (Fig. 1a); of note, the small peak at m/z 6057 Da is a fragment (i.e., $Au_{21}(SR)_{14}$) caused by the somewhat destructive MALDI method, in consistent with the reported literatures [25]. No other peaks were found, indicating the purity of the $Au_{25}(SR)_{18}$ nanoclusters. Similarly, the single peak at m/z 7392 Da for the $Pt_1Au_{24}(SR)_{18}$ nanocluster indicates the product purity [6]. However, the cases of Ag and Cu doping did not give rise to singly doped nanoclusters, instead, a distribution of $Ag_xAu_{25-x}(SR)_{18}$ or $Cu_xAu_{25-x}(SR)_{18}$. As shown in Fig. 1c, the spacing of the $Ag_xAu_{25-x}(SR)_{18}$ peaks is 89–90 Da, indicating the atomic mass difference between gold and silver (M_{Au}–M_{Ag}=197.0–107.9=89.1 Da), suggesting that gold atoms were successively replaced by silver atoms, but the total metal atoms of the cluster were preserved at 25. The maximum doping number of the $Ag_xAu_{25-x}(SR)_{18}$ nanoclusters was up to five, Fig. 1c, inset. Similarly, in the case of $Cu_xAu_{25-x}(SR)_{18}$ (Fig. 1d), the peak spacing was 133–134 Da (theoretical M_{Au}–M_{Cu}=197.0–63.5=133.5 Da), indicating the substitution of gold for copper. And the maximum replacement in $Cu_xAu_{25-x}(SR)_{18}$ was six, as shown in Fig. 1d, inset. Of note, similar with the cases of $Au_{25}(SR)_{18}$ and $Pt_1Au_{24}(SR)_{18}$ nanoclusters, a serial of fragments, noted as asterisks, were found in the $Cu_xAu_{25-x}(SR)_{18}$ and $Ag_xAu_{25-x}(SR)_{18}$ (Fig. 1c and d).

3.2. Characterization of the TiO_2-supported $M_xAu_{25-x}(SR)_{18}$ catalysts

These different bimetallic gold-based nanoclusters were supported on TiO_2, and then used as catalysts in the carbon–carbon coupling reaction system. The oxide-supported bimetallic gold-based nanoclusters $M_xAu_{25-x}(SR)_{18}$ catalysts were made by impregnation of the TiO_2 oxide powders in a dichloromethane (DCM) solution of $M_xAu_{25-x}(SR)_{18}$ nanoclusters, and then annealed at 150 °C (1 h) in a vacuum oven [20]. The TiO_2-supported $Au_{25}(SR)_{18}$ catalyst was still intact after the annealing process, which is supported by the Z-contrast scanning transmission electron microscopy and thermogravimetric analysis in our previous work [20]. And more, no discernable loss of ligands of the pure $Au_{25}(SR)_{18}$ nanoclusters showed during the thermal stability analysis (e.g., at 150 °C in air atmosphere for 1 h) [20]. The external staples of the bimetallic gold-based nanoclusters $M_xAu_{25-x}(SR)_{18}$ catalysts were exclusively $Au_2(SR)_3$, therefore we believe that the other oxide-supported bimetallic nanoclusters $M_xAu_{25-x}(SR)_{18}$ should also remain stable after the thermal treatments.

Next, the surface gold and transition metal atoms of the $M_xAu_{25-x}(SR)_{18}/TiO_2$ (where, M=Pt, Cu, and Ag) catalysts were characterized by XPS analysis, as seen in Fig. 2. The XPS spectra of the $Ag_xAu_{25-x}(SR)_{18}$ show the binding energies (BEs) of Au $4f_{7/2}$ and Au $4f_{5/2}$ are at 83.70 and 87.38 eV and the BEs of Ag $3d_{5/2}$ and Ag $3d_{3/2}$ are at 367.43 and 373.61 eV (Fig. 2A and B). Meanwhile, the BEs of the Au $4f_{7/2}$, Au $4f_{5/2}$, and Cu 2p of $Cu_xAu_{25-x}(SR)_{18}$ nanoclusters are located at 83.65, 87.33, and 932.06 eV, respectively (Fig. 2C and D). And in the case of $PtAu_{24}(SR)_{18}$ nanoclusters, the BEs of the Au $4f_{7/2}$,

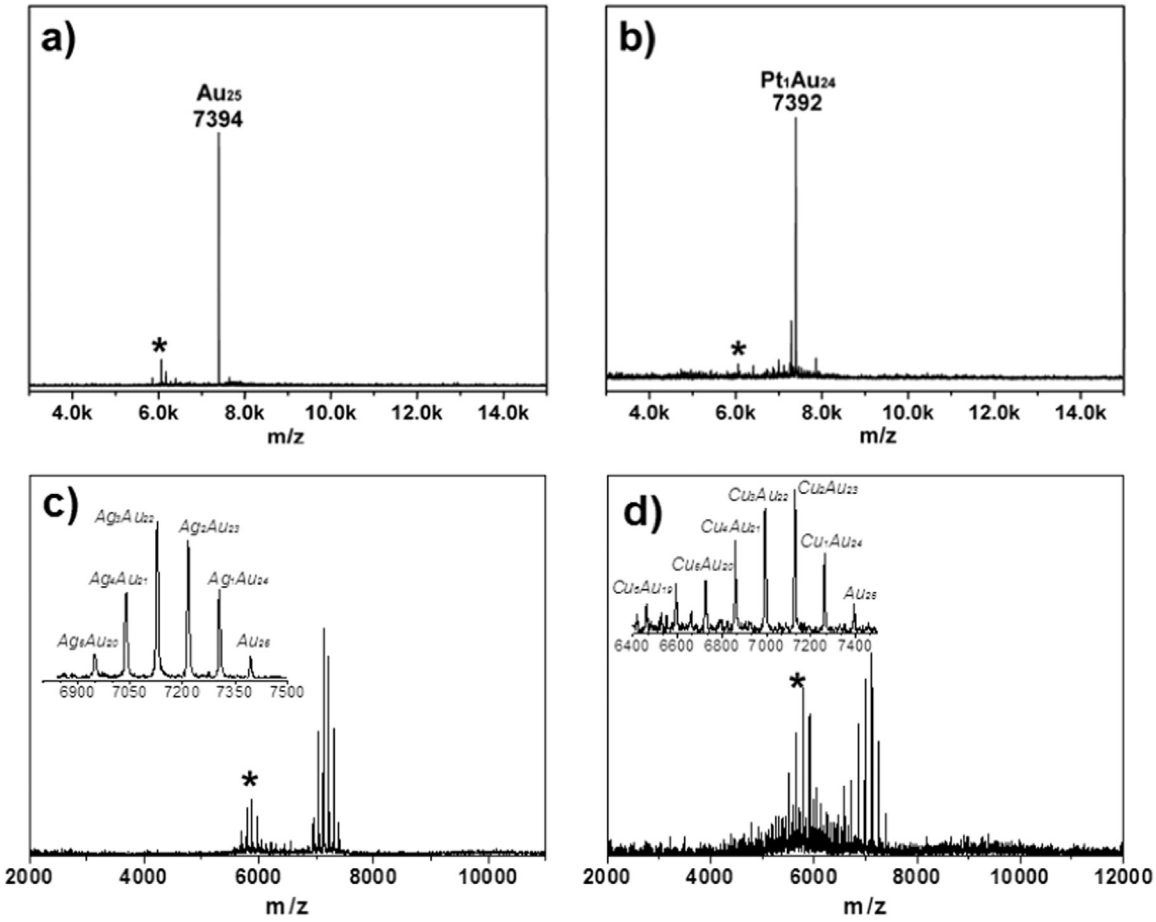

Fig. 1. MALDI mass spectra of the four nanoclusters: (a) $Au_{25}(SR)_{18}$, (b) $Pt_1Au_{24}(SR)_{18}$, (c) $Ag_xAu_{25-x}(SR)_{18}$ (x=0 to 5), and (d) $Cu_xAu_{25-x}(SR)_{18}$ (x=0 to 6). The insets in (c) and (d) are the zoom-in spectra. The asterisks (*) stand for the fragments of these nanoclusters caused by the some destructive MALDI method. –SR=–SCH_2CH_2Ph.

Au $4f_{5/2}$, Pt $4f_{7/2}$, and Pt $4f_{5/2}$ are 83.50, 87.48, 71.81, and 75.05 eV, respectively, as shown in Fig. 2E and F. These shifts of ca. 0.1–0.3 eV toward the binding energy of the natural metallic Au (Au$4f_{7/2}$: 83.8 eV) may be attributable to charge transfer between Au and metal species (Au, Ag, and Pt), indicating that the electronic structure of the clusters was modified by dopants.

3.3. Catalytic performance of the gold-based bimetallic nanoclusters in carbon–carbon coupling reaction

Next, we choosed *p*-iodoanisole and phenylacetylene as reactants for the caborn–carbon coupling reaction. In general, the reaction between *p*-iodoanisole and phenylacetylene (Scheme 1) usually give rise to two main homo-coupling products (diphenyldiacetylene and 4,4′-dimethoxy-1,1′-biphenyl) and a Sonogashira cross-coupling product (1-methoxy-4-(2-phenylethynyl)benzene) [26–28]. The catalytic reaction was carried out at 160 °C for 40 h under a N_2 atmosphere; other conditions were 0.1 mmol *p*-iodoanisole, 0.1 mmol phenylacetylene, 0.3 mmol potassium carbonate (K_2CO_3), 1 mL *N*, *N*′-dimethylformamide (DMF), and 100 mg $M_xAu_{25-x}(SR)_{18}$/oxide catalyst (the net amount of bimetallic nanoclusters: 1 mg), the details can be seen in the Experimental section. The reaction products were analyzed by ^1H NMR spectroscopy.

When $Au_{25}(SR)_{18}/TiO_2$ was used as the catalyst in the carbon–carbon coupling reaction, we obtained 79.5% conversion of *p*-iodoanisole and 65.7% selectivity for the cross-coupling product MPEB (Table 1, entry 1); hereafter, the conversion is based on *p*-iodoanisole and the selectivity is for MPEB. We then tested the catalytic activities of the other three gold-based bimetallic nanoclusters catalysts. When using $Ag_xAu_{25-x}(SR)_{18}/TiO_2$ as the catalyst (Table 1, entry 2), the conversion (83.0%) was slightly higher than that of $Au_{25}(SR)_{18}/TiO_2$, but the selectivity was much lower (55.4% with Ag-doped catalyst vs. 65.7% with homogold catalyst). We further investigated $Cu_xAu_{25-x}(SR)_{18}/TiO_2$ and $Pt_1Au_{24}(SR)_{18}/TiO_2$ (Table 1, entry 3 and 4). In both cases, the conversion decreased to 52.4% and 48.5%, respectively, but the selectivity was drastically different (28.3% with $Cu_xAu_{25-x}(SR)_{18}/TiO_2$ and 67.2% with $Pt_1Au_{24}(SR)_{18}/TiO_2$). Based on the conversion, the catalytic performance of the titania-supported catalysts follows the following decreasing order:

$Ag_xAu_{25-x}(SR)_{18} \approx Au_{25}(SR)_{18} > Cu_xAu_{25-x}(SR)_{18} > Pt_1Au_{24}(SR)_{18}$.

In terms of the selectivity, $Cu_xAu_{25-x}(SR)_{18}/TiO_2$ was contrary with $Au_{25}(SR)_{18}/TiO_2$ and $Pt_1Au_{24}(SR)_{18}/TiO_2$, which implies that the $Cu_xAu_{25-x}(SR)_{18}/TiO_2$ catalyst prefers the Ullmann homo-coupling process, while the latter two catalysts give predominant cross-coupling. On the other hand, $Ag_xAu_{25-x}(SR)_{18}/TiO_2$ gives rise to no preference of the cross-coupling over the Ullmann homo-coupling.

3.4. Mechanism of the carbon–carbon coupling reaction

Taken together, the above catalytic results of bimetallic nanoclusters catalysts exhibit distinct effects of doping atoms on the catalytic activity and selectivity in the carbon–carbon coupling reaction between *p*-iodoanisole and phenylacetylene. Furthermore, the correlation of the catalytic performance with the cluster structure and electronic properties will be discussed.

The $[Au_{25}(SR)_{18}]^-TOA^+$(TOA=tetraoctylammonium) nanoclusters [24] possesses a core/shell $Au_{13}@Au_{12}(SR)_{18}$ structure. The Au_{13} core consists of one center and an icosahedral shell of 12 atoms, whereas the

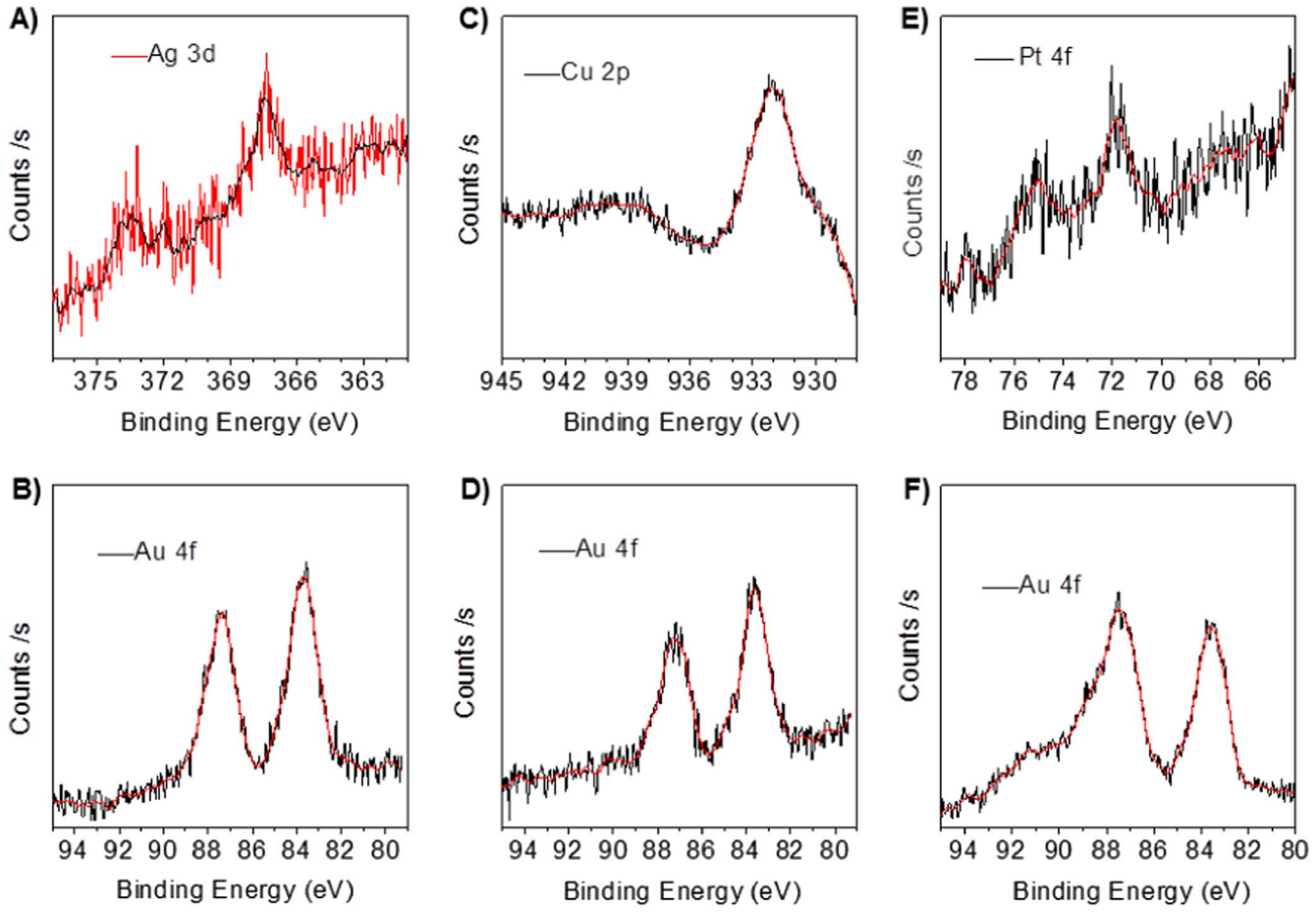

Fig. 2. XPS spectra of $M_xAu_{25-x}(SR)_{18}$ catalysts. (A) Au 4f and (B) Ag 3d for $Ag_xAu_{25-x}(SR)_{18}$; (C) Au 4f and (D) Cu 2p for $Cu_xAu_{25-x}(SR)_{18}$; (E) Au 4f and (F) Pt 4f for $Pt_1Au_{24}(SR)_{18}$.

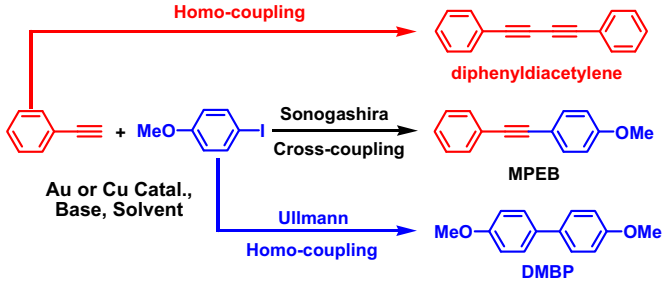

Scheme 1. Catalytic carbon–carbon coupling reaction of *p*-iodoanisole and phenylacetylene to yield the Sonogashira cross-coupling product 1-methoxy-4-(2-phenylethynyl) benzene (MPEB) and two homo-coupling products 4,4′-dimethoxy-1,1′-biphenyl (DMBP) and diphenyldiacetylene.

exterior $Au_{12}(SR)_{18}$ shell can be viewed as six –S(R)-Au-S(R)-Au-S(R)– semirings (so called dimeric staple motifs). In general, the foreign atoms could reside in three types of atomic positions in the structure, that is, in the icosahedral center (only one available site), in the Au_{12} icosahedral shell (12 metal atom sites total), or in the exterior dimeric staples (12 metal atom sites total). In our previous work on the $Pt_1Au_{24}(SR)_{18}$ nanoclusters, both experiment and theory confirmed that the single Pt atom is located at the center of the 25-metal-atom cluster, $Pt_1@Au_{12}@Au_{12}(SR)_{18}$ [6]. In contrast, for both $Ag_xAu_{25-x}(SR)_{18}$ and $Cu_xAu_{25-x}(SR)_{18}$, the multiple copper and silver dopant atoms are preferentially located in the icosahedral Au_{12} shell, instead of the exterior $Au_{12}(SR)_{18}$ shell [29,30]. The interesting different distributions of the two metallic components in the gold-based bimetallic nanoclusters may significantly alter the catalytic performance of the oxide-supported catalyst.

The carbon-carbon coupling reactions (the MeOPhI/PhC≡CH pair, MeOPhI/MeOPhI pair, and PhC≡CH/PhC≡CH pair) yield the cross-coupling product MPEB, and homo-coupling products DMBP and diphenyldiacetylene, respectively (Scheme 1). The co-adsorption energies of the PhI/PhC≡CH pair, PhI/PhI pair, and PhC≡CH/PhC≡CH pair on the surface of the model $Au_{25}(SCH_2CH_2Ph)_{18}$ nanocluster catalyst have previously been calculated by density functional theory (DFT) method [20]. In the DFT calculations, the *p*-iodoanisole (MeOPhI) was replaced by iodobenzene (PhI) to reduce computational demand. It was found that the PhC≡CH/PhC≡CH pair and PhI/PhI pair have a co-adsorption energy of −0.90 eV and −1.05 eV (negative means stabilization), respectively. On the other hand, the PhC≡CH/PhC≡CH pair has an adsorption energy of −0.86 eV. The DFT calculation result indicates that the PhI/PhI pair seems easier adsorbed and interacts slightly stronger with the $Au_{25}(SCH_2CH_2Ph)_{18}$ nanocluster catalyst than other two pairs, PhC≡CH/PhC≡CH and PhI/PhC≡CH; of note, phenylacetylene or/and iodobenzene adsorbs on one gold atom, the other reactant adsorbs on the second gold atom, and both the –C≡CH or/and –I groups point towards the third external gold atom and even bond to the sub-surface of the Au_{13} icosahedral core (Scheme 2).

Based on the above experimental and DFT results, we propose a mechanism for the $M_xAu_{25-x}(SR)_{18}$ catalyzed Sonogashira cross-coupling reaction of phenylacetylene and *p*-iodoanisole. It is worthy of noting that the $M_xAu_{25-x}(SR)_{18}$ nanoclusters [29,30] share the same structure as that of the $Au_{25}(SR)_{18}$ nanocluster, but the external staples are exclusively $Au_2(SR)_3$, while the icosahedral surface is composed of both Au and Ag (or Cu) atoms in $Ag_xAu_{25-x}(SR)_{18}$ and $Cu_xAu_{25-x}(SR)_{18}$; in contrast, the single Pt atom is located in the icosahedral center of $Pt_1Au_{24}(SR)_{18}$. Thus, we use the crystal structure of $Au_{25}(SR)_{18}$ nanoclusters as the model in the proposed mechanism of

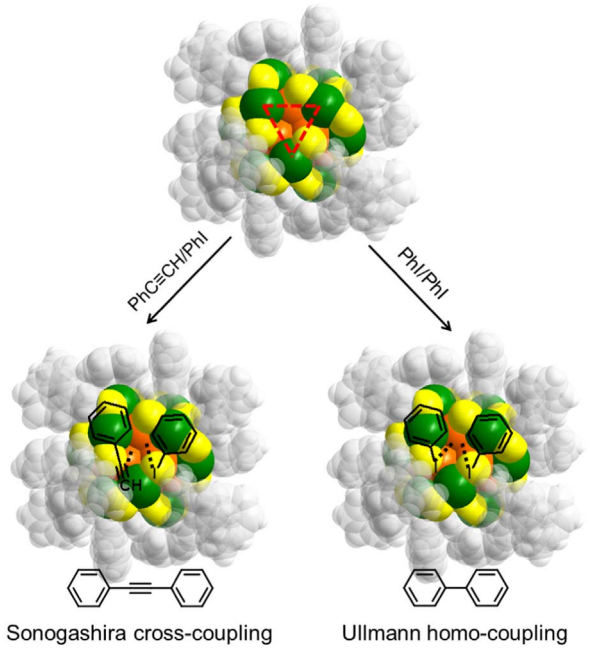

Scheme 2. The proposed mechanism for the $M_xAu_{25-x}(SR)_{18}$ catalyzed-coupling reaction of the iodobenzene and phenylacetylene. The PhC≡C-H/pH-I (left panel) and pH-I/pH-I (right panel) pairs are adsorbed on the Au_3 open facet, which leads to Sonogashira cross-coupling and Ullmann homo-coupling reactions. The $Au_{25}(SR)_{18}$ structure is drawn in the space-filling mode and is used as the model for the $M_xAu_{25-x}(SR)_{18}$ nanoclusters. Color code: gold atoms on the staple motif ($Au_{12}(SR)_{18}$), green; metal atoms on M_{13} icosahedral core, orange; sulfur atoms, yellow; carbon atoms, grey; hydrogen atoms, white. Of note, the *p*-iodoanisole was replaced by iodobenzene (PhI) for clarity.

the Sonogashira cross-coupling reaction catalyzed $M_xAu_{25-x}(SR)_{18}$ nanoclusters (Scheme 2). In the previous literautes, the catalytic reactions are speculate to occur on the open facet of gold nanoclusters [20,31,32]. Initially, the *p*-iodoanisole and phenylacetylene molecules are adsorbed onto the open facet (i.e., the triangular Au_3 surface motif) of $M_xAu_{25-x}(SR)_{18}$ nanocluster catalysts, and then the reactants interact with each other and become activated through interactions with both the external Au_3 and the metal atoms (i.e., Au, Ag, and Cu) on the surface of the M_xAu_{13-x} icosahedral core in the presence of the base (e.g., K_2CO_3, as shown in Scheme 2). The Ph-I bond would be activated to the Ph···Au···I intermediate. Meanwhile, the C-H bond of phenylacetylene can be activated to the Au···C≡CPh intermediate. These intermediates on the adjacent metal atoms can couple with each other to form the cross-coupling product (1-methoxy-4-(2-phenylethynyl)benzene) and homo-coupling products (4,4′-dimethoxy-1,1′-biphenyl and diphenyldiacetylene).

The above experimental results imply that the catalytic activity was determined by the electronic effects of the $M_xAu_{25-x}(SR)_{18}$ nanoclusters and the atom type on the surface of M_xAu_{13-x} icosahedral core. On the other hand, the selectivity was dominated by the atom type on the surface of M_xAu_{13-x} icosahedral core in the competing coupling reaction of the MeOPhI/PhC≡CH pair and MeOPhI/MeOPhI pair (Scheme 2).

Control experiments using plain oxide powders gave no conversions of iodoanisole and phenylacetylene under the identical reaction conditions. Thus, the carbon–carbon coupling reaction of iodoanisole and phenylacetylene is catalyzed by the bimetallic nanoclusters, especial by the 13-atom icosahedral core of the bimetallic nanoclusters. The oxide-supported $Au_{25}(SR)_{18}$ nanocluster catalyst exhibits better catalytic activity than $Pt_1Au_{24}(SR)_{18}$ nanoclusters in terms of the conversion of iodoanisole, but these two catalysts show similar selectivity for MPEB product. The observed similar selectivity is reasonable since both $Pt_1Au_{24}(SR)_{18}$ and $Au_{25}(SR)_{18}$ have the same types of surface atoms (all are Au atoms); the reduced activity of $Pt_1Au_{24}(SR)_{18}$ should be caused by potential electron density transfer from the Au_{12} shell to the central Pt atom.

When comparing the catalytic performance of $Ag_xAu_{25-x}(SR)_{18}$ with that of $Au_{25}(SR)_{18}$, the most distinct difference lies in the selectivity for MPEB product. The presence of Ag dopant atoms in the M_{12} icosahedral shell seems not favourable for the selectivity to MPEB. Similarly, the presence of Cu dopants also significantly reduces the selectivity for MPEB. Another potential factor for the lower activity and selectivity of the $Cu_xAu_{25-x}(SR)_{18}$ catalyst is its less stability compared to $Ag_xAu_{25-x}(SR)_{18}$ and $Au_{25}(SR)_{18}$.

The $Cu_xAu_{25-x}(SR)_{18}$ catalyst is very interesting that the selectivity for MPEB is indeed completely reversed (i.e., favoring the Ullmann homo-coupling pathway) compared to the $Ag_xAu_{25-x}(SR)_{18}$, $Pt_1Au_{24}(SR)_{18}$, and $Au_{25}(SR)_{18}$ nanocluster catalysts that favor the cross-coupling product. Of note, copper complexes and nanoclusters are well known excellent catalysts for the Ullmann homo-coupling reaction [33,34]. In our system, the reversed selectivity of $Cu_xAu_{25-x}(SR)_{18}$ for Ullmann homocoupling can be accounted for by the rich Cu contents in the icosahedral shell of Cu_xAu_{13-x}. To further confirm that, we synthesized small-size thiolate-capped copper nanoclusters $Cu_n(SR)_m$ with the same thiol ligand (phenylethanethiol) by a synthetic method similar to that of $Au_{25}(SR)_{18}$. Under the identical carbon–carbon coupling reaction condition, the $Cu_n(SR)_m/TiO_2$ catalyst gave 71.4% conversion, and 21.4% selectivity for the cross-coupling product (MPEB), and 78.6% selectivity for the Ullmann homo-coupling product (DMBP). This catalytic result implies that the TiO_2-supported copper nanocluster catalyst prefers to yield Ullmann homo-coupling product in the carbon–carbon coupling reaction of iodoanisole and phenylacetylene. Compared to the MeOPhI/PhC≡CH pair, the MeOPhI/MeOPhI pair interacts more strongly with the external Au_3 and the copper atoms on the surface of the Cu_xAu_{13-x} icosahedral core.

4. Conclusions

In summary, we have investigated the catalytic activity of gold-based bimetallic $M_xAu_{25-x}(SR)_{18}$ (M=Pt, Cu, and Ag) nanoclusters supported on titania for the reaction of carbon–carbon coupling of *p*-iodoanisole and phenylacetylene. The titania-supported $Au_{25}(SR)_{18}$ nanoclusters exhibit better catalytic performance (conversion of the *p*-iodoanisole and selectivity for the Sonogashira cross-coupling product 1-methoxy-4-(2-phenylethynyl)benzene) than other bimetallic $M_xAu_{25-x}(SR)_{18}$ nanoclusters. Compared to homogold $Au_{25}(SR)_{18}$, the centrally doped $Pt_1Au_{24}(SR)_{18}$ causes a drop in catalytic activity but with the selectivity retained, while the $Ag_xAu_{25-x}(SR)_{18}$ nanoclusters gave an overall performance comparable to $Au_{25}(SR)_{18}$. Interestingly, $Cu_xAu_{25-x}(SR)_{18}$ nanoclusters prefer the Ullmann homo-coupling pathway and give rise to product 4,4′-dimethoxy-1,1′-biphenyl, which is in opposite to the other three nanocluster catalysts. Our overall conclusion is that the conversion of *p*-iodoanisole is largely affected by the electronic effect in the bimetallic nanoclusters' 13-atom core (i.e., Pt_1Au_{12}, Cu_xAu_{13-x}, and Au_{13}, with the exception of Ag doping), and that the selectivity is primarily determined by the type of atoms on the M_xAu_{12-x} (M=Ag, Cu, and Au) shell in the nanocluster catalysts.

Acknowledgement

This work was financially supported by the scholarship support from the starting fund of the "Thousand Youth Talents Plan".

References

[1] C.L. Bracey, P.R. Ellis, G.J. Hutchings, Chem. Soc. Rev. 38 (2009) 2231.
[2] B.R. Cuenya, Acc. Chem. Res. 46 (2013) 1682.

[3] R.M. Anderson, D.F. Yancey, L. Zhang, S.T. Chill, G. Henkelman, R.M. Crooks, Acc. Chem. Res. 48 (2015) 1351.
[4] G. Li, R. Jin, Nanotechnol. Rev. 5 (2013) 529.
[5] S. Xie, H. Tsunoyama, W. Kurashige, Y. Negishi, T. Tsukuda, ACS Catal. 2 (2012) 1519.
[6] H. Qian, D. Jiang, G. Li, C. Gayathri, A. Das, R.R. Gil, R. Jin, J. Am. Chem. Soc. 134 (2012) 16159.
[7] W. Li, C. Liu, H. Abroshan, Q. Ge, X. Yang, H. Xu, G. Li, J. Phys. Chem. C 120 (2016) 10261.
[8] N.K. Chaki, H. Tsunoyama, Y. Negishi, H. Sakurai, T. Tsukuda, J. Phys. Chem. C 111 (2007) 4885.
[9] G. Li, R. Jin, Catal. Today (2016). http://dx.doi.org/10.1016/j.cattod.2015.11.019.
[10] B.N. Wanjala, J. Luo, B. Fang, D. Mott, C.-J. Zhong, J. Mater. Chem. 21 (2011) 4012.
[12] K. Kaizuka, H. Miyamura, S. Kobayashi, J. Am. Chem. Soc. 132 (2010) 15096.
[13] F. Monnier, M. Taillefer, Angew. Chem. Int. Ed. 48 (2009) 6954.
[14] G. Evano, N. Blanchard, M. Toumi, Chem. Rev. 108 (2008) 3054.
[15] J. Lin, H. Abroshan, C. Liu, M. Zhu, G. Li, M. Haruta, J. Catal. 330 (2015) 354.
[16] Y. Chen, C. Liu, H. Abroshan, J. Wang, Z. Li, G. Li, M. Haruta, J. Catal. 337 (2016) 287.
[17] P. Venkatesan, J. Santhanalakshmi, Langmuir 26 (2010) 12225.
[18] G. Li, R. Jin, Acc. Chem. Res. 46 (2013) 1749.
[19] G. Li, C. Liu, Y. Lei, R. Jin, Chem. Commun. 48 (2012) 12005.
[20] G. Li, D. Jiang, C. Liu, C. Yu, R. Jin, J. Catal. 306 (2013) 177.
[21] H. Abroshan, G. Li, J. Lin, H.J. Kim, R. Jin, J. Catal. 337 (2016) 72.
[22] G. Li, H. Abroshan, C. Liu, S. Zhuo, Z. Li, Y. Xie, H.J. Kim, N.L. Rosi, R. Jin, ACS Nano (2016). http://dx.doi.org/10.1021/acsnano.6b03964.
[23] E. Gottlieb, H. Qian, R. Jin, Chem. Eur. J. 19 (2013) 4238–4243.
[24] M. Zhu, C.M. Aikens, F.J. Hollander, G.C. Schatz, R. Jin, J. Am. Chem. Soc. 130 (2008) 5883.
[25] J. Lin, W. Li, C. Liu, P. Huang, M. Zhu, Q. Ge, G. Li, Nanoscale 7 (2015) 13663.
[26] T. Tabakova, F.B. Boccuzzi, M. Manzoli, D. Andreeva, Appl. Catal. A: Gen. 252 (2003) 385.
[27] A. Bensalem, F. Bozon–Verduraz, React. Kinet. Catal. Lett. 60 (1997) 71.
[28] S. Bernal, J.J. Calvino, G.A. Cifredo, J.M. Rodriguez–Izquierdo, V. Perrichon, A. Laachir, J. Catal. 137 (1992) 1.
[29] D. Jiang, S. Dai, Inorg. Chem. 48 (2009) 2720.
[30] Y. Negishi, K. Munakata, W. Ohgake, K. Nobusada, J. Phys. Chem. Lett. 3 (2012) 2209.
[31] C. Yan, C. Liu, H. Abroshan, Z. Li, R. Qiu, G. Li, Phys. Chem. Chem. Phys. 18 (2016) 23358.
[32] G. Li, R. Jin, J. Am. Chem. Soc. 136 (2014) 11347.
[33] T.D. Nelson, R.D. Crouch, Org. React. 63 (2004) 265.
[34] F. Monnier, M. Taillefer, Angew. Chem. Int. Ed. 47 (2008) 3096.